

Synthesis of Micro/nanostructured Carbon from Refined Sugar and its Electrochemical Performance

D. Macías-Ferrer^{1*}, J.A. Melo-Banda¹, R. Silva-Rodrigo¹, U. Páramo-García¹, J.Y. Verde-Gómez², P. Del-Angel-Vicente³

¹ Division of Postgraduate Studies and Research, Technological Institute of Cd. Madero, Cd. Madero, Tamaulipas, 89440, México

² Division of Postgraduate Studies and Research, Technological Institute of Cancún, Cancún, Quintana Roo, 77500, México

³ Laboratory of Characterization of Natural and Synthetic Materials, Mexican Institute of Petroleum, Mexico City, 07730, México

*E-mail: maestro_macias@hotmail.com

Received: 9 September 2017 / Accepted: 16 November 2017 / Published: 16 December 2017

Micro/nano-structured carbon (MNC) was synthesized using nanocasting method and anhydrous pyrolysis process at 1000 °C using refined sugar as carbon precursor and SBA-15 as structure directing agent. SBA-15 was prepared through sol gel using the copolymer triblock non ionic pluronic P-123 as surfactant and tetraethyl orthosilicate as Si precursor. The prepared materials were characterized by means of N₂ physisorption, Fourier transform infrared spectroscopy (FTIR), X-ray diffraction (XRD), Raman spectroscopy, scanning electron microscopy (SEM), energy-dispersive X-ray spectroscopy (EDS), high resolution transmission electron microscopy (HRTEM) and cyclic voltammetry (CV). The applied characterization techniques revealed that MNC has a mesoporous and turbostratic structure with rope like morphology composed by a set of carbon nanofibers and carbon nanopipes wrapped by thin graphene layers with large specific surface area (1292 m²/g) and large pore volume (1.2 cc/g), so MNC is a promising material for applications in adsorption, energy storage and solar cells, supercapacitor electrodes and electrocatalytic supports.

Keywords: SBA-15, nanocasting, carbon nanopipes, carbon nanofibers, turbostratic carbon

1. INTRODUCTION

According with the International Union of Pure and Applied Chemistry (IUPAC), porous materials are divided into three classes: microporous (< 2 nm), mesoporous (2–50 nm) macroporous (> 50 nm) [1-2]. Porous carbon materials have generated tremendous interest in many areas of science and technology because of their excellent chemical, thermal and mechanical stability, electrochemical

capacitive ability, electrical conductivity, chemical inertness, high specific area and large pore volume. Due to their properties, these materials have been used in adsorption, catalysis, electrocatalysis, supercapacitors, biomedical engineering, energy conversion and storage [3-8]. With the discovery of both fullerene (1985) and carbon nanotubes (1991), many research has focused on the development of new mesoporous carbon materials such as carbon nanocages (CNC's), carbon nanofibers (CNF's), carbon nanospheres (CNC's) and graphene [9-15]. According with structural ordering, mesoporous carbon can be divided in two classes: Ordered mesoporous carbon (OMC) and disordered mesoporous carbon (DMC) [16-18]. From 1991, the nanocasting process has attracted more attention and become one of the most important approaches for the synthesis of porous materials, especially mesoporous materials [19-20]. Materials such as anodic aluminum oxide, zeolite, silica opal, phenolic resin [21-25], 2-D mesostructured materials with hexagonal symmetry such as Mobil Composition of Matter No. 41 (MCM-41) and No. 48 (MCM-48), Folded Sheets Mesoporous Material No. 16 (FSM-16), Korea Institute of Technology No. 6 (KIT-6) and Santa Barbara Amorphous No. 15 (SBA-15) have been used as templates to produce ordered mesoporous carbon materials with high specific surface area S_{BET} [26-29]. Many types of carbon precursors such as phenol-formaldehyde, glycerol, furfuryl alcohol, sucrose [30-33], have been used in order to obtain nanostructured carbon with the method mentioned above. In this study, We have synthesized the MNC material by nanocasting method in accordance with literature reported, with the particularity of handling an excess quantity of refined sugar in order to create layers of graphene that hold together both carbon nanofibers and carbon nanopipes after silica removal process.

2. EXPERIMENTAL

2.1 Chemicals

Pluronic P-123 (non-ionic triblock copolymer, $\text{EO}_{20}\text{PO}_{70}\text{O}_{20}$), tetraethoxysilane ($\text{Si}(\text{OC}_2\text{H}_5)_4$, 98%), graphite powder (C, 99.99%), graphitized carbon black (C, 99.95%) and Nafion[®] 117 solution (5% wt) were obtained from Sigma-Aldrich; deionized water, hydrochloric acid (HCl, 37%) and sodium hydroxide (NaOH, 97%) and sulfuric acid (H_2SO_4 , 99%), were supplied by Fermont and refined sugar (sucrose, 96%) were obtained by Del Marques S.A.

2.2 Synthesis of MNC

SBA-15 samples were synthesized according to the standard procedure [34-35] with some modifications. In a typical synthesis, 2.0 g Pluronic P-123 as a structure-directing agent were dissolved in 14 mL ultrapure water and 60 mL 0.6 M hydrochloric acid by stirring at room temperature for 5 h. Afterwards, 4.3 mL of tetraethoxysilane (TEOS) were added dropwise and the mixture was stirred (700 rpm) at 45 °C for 24 h in the closed glass reactor. Subsequently the mixture is aged in oven at 90 °C for 24 h. The white powder was obtained through filtration, washing and drying in nalgene bottle under vacuum. Finally, the sample was calcined at 550 °C for 6 h under air to remove the surfactant to obtain the silica template. MNC was prepared by nanocasting method [36-37]. Briefly, 1.2 g of refined

sugar and 1 g of SBA-15 were dissolved in 5 mL of deionized water by stirring at room temperature for 30 min, during this time 0.05 mL of sulfuric acid was added. The mixture was heated in an oven at 100 °C for 6 h, and subsequently 160 °C for another 6 h. The dark brown powder (Suc-SBA15) was carbonized in a quartz furnace at 1000 °C for 1 h under N₂ flow. Finally, the silicon removal was carried out under vigorous stirring using a solution 2M NaOH for 24 h and subsequently filtered, washed and dried in a oven for 12 h.

2.3 Characterization of materials

The textural properties of the samples were analyzed by N₂ adsorption/desorption on a Quantachrome model Autosorb-iQ ASIQA0000-2 at 77K. The S_{BET} and pore size distributions (PSDs) of the samples were calculated according to the Brunauer–Emmet–Teller method and Barrett–Joyner–Halenda equation. X-ray powder diffraction (XRD) patterns were collected on a Bruker D8 Advance X-ray diffractometer with Cu K α radiation ($\lambda = 0.154$ nm) to verify the formation of products and the small-angle X-ray scattering (SAXS) technique on a Siemens D500 X-ray diffractometer. The Raman measurements were carried out using a Bruker model Raman-Senterra spectrometer with Olympus BX microscope and Ar laser (785 nm). In order to determine the morphology and the average chemical composition of the samples, scanning electron microscopy (SEM) and energy dispersive X-ray characterizations were performed using a JEOL model JSM-7100F operating at 20 KeV with EDS detector from Oxford Instruments. The high resolution transmission electron microscopy (HR-TEM) is performed using a JEOL JEM-2200FS with Schottky type field emission gun (FEG) with point image resolution of 0.19 nm, and slow scan CCD camera Gatan Co.

2.4 Electrochemical measurements

The electrochemical performance of micro/nanostructured carbon and commercial carbon Vulcan XC-72 commercial carbon powder at room temperature was evaluated by cyclic voltammetry (CV) using a BASi epsilon electrochemical analyzer with a conventional three-electrode cell consisting of the glassy carbon (GC, 0.0707 cm²) as working electrode, the coiled Pt wire auxiliary electrode and Ag/AgCl as reference electrode. The working electrode was prepared as follows. A glassy carbon electrode was sequentially polished with 0.05 μm -sized Al₂O₃ and then washed. The carbon material ink was formed by ultrasonically dispersing 10 mg of active material into a solution consisting 94.4 % ethanol, 4.2 % water and 1.4 % Nafion. 10 μL of this mixture was transferred onto glassy carbon, after drying at 40°C for 30 min the working electrode is obtained. A solution of 0.5 M H₂SO₄ was used for electrochemical measurement. Highly pure N₂ was used prior to the measurements to remove O₂ that is dissolved in the electrolyte. Cyclic voltammetric measurements of MNC and Vulcan XC-72 were carried out at a scan rate of 20 mV/s and a scan scope of -0.2 V to 1.0 V.

3. RESULTS AND DISCUSSION

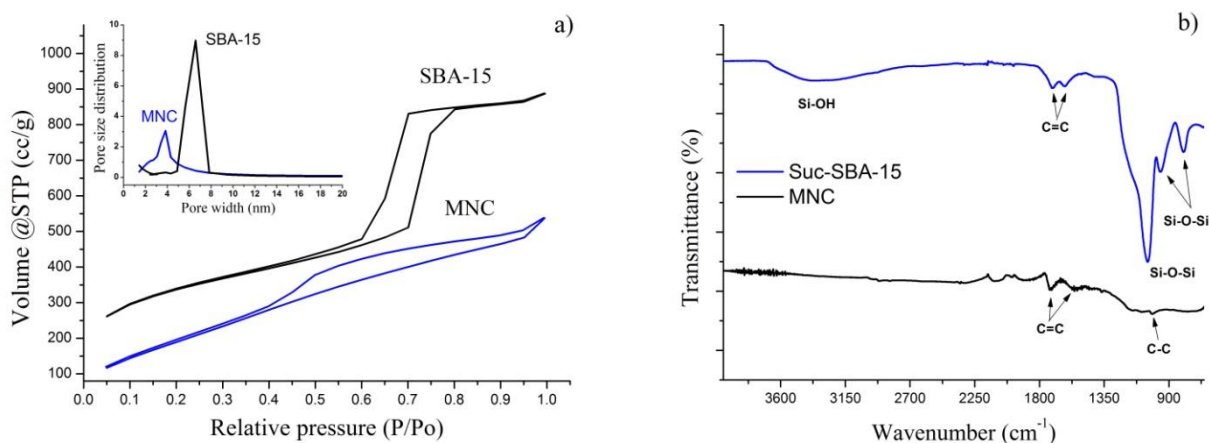


Figure 1. a) N_2 adsorption-desorption isotherms and the pore diameter distribution (inset) of the SBA-15 and MNC; b) FTIR spectra of Suc-SBA-15 and MNC.

Fig. 1a shows the N_2 adsorption/desorption isotherms of the SBA-15 and MNC after removal silicon; both samples show typical type IV isotherms with significant H1 (SBA-15) and H4 (MNC) hysteresis loops, respectively [38]. The BJH pore size distributions of the samples are shown in the inset. The mesoporous carbon particles have a pore size distribution centered at 3.8 nm while the mesoporous silica particles have a pore size distribution centered at 7.8 nm. The S_{BET} for the silica particles and MNC were $872 \text{ m}^2/\text{g}$ and $1192 \text{ m}^2/\text{g}$ respectively. The pore volume of the silica templates and resulting carbon particles are 0.97 and 1.2 cc/g, respectively. The FTIR spectra of the nanocomposite Suc-SBA-15 and MNC after pyrolysis at 1000°C in Fig. 1b are illustrated.

For Suc-SBA-15 nanocomposite, appear the weak and broad band at 3333 cm^{-1} attributed to the stretching vibrations of the surface silanol groups Si-OH and the remaining adsorbed water molecules in O-H bond, the typical Si-O-Si band at 1048 cm^{-1} associated to antisymmetric vibrations (this band also could be related to stretching vibrations of Si-O-C, C-O-O and Si-C overlapped with Si-O-Si), the Si-O-Si bands ($960, 798 \text{ cm}^{-1}$) related to symmetric and bending stretching vibrations respectively, all of them associated with the formation of a condensed silica network [39-40]. Furthermore, two absorption bands at around 1714 cm^{-1} and 1618 cm^{-1} that correspond to stretching vibration of double bond C=C in the aromatic structures due to carbon into silica pores. For MNC after silica removal process, appear again two absorption bands at around 1714 cm^{-1} and 1571 cm^{-1} that corresponds to stretching vibration of the carbon double bond C=C. The band at around 1714 cm^{-1} , also could be related to stretching vibrations of C=O overlapped with C=C. MNC also shows a weak band at around 1019 cm^{-1} that corresponds to stretching vibrations of C-C bond, finally, absorption bands related with silica not appear [41].

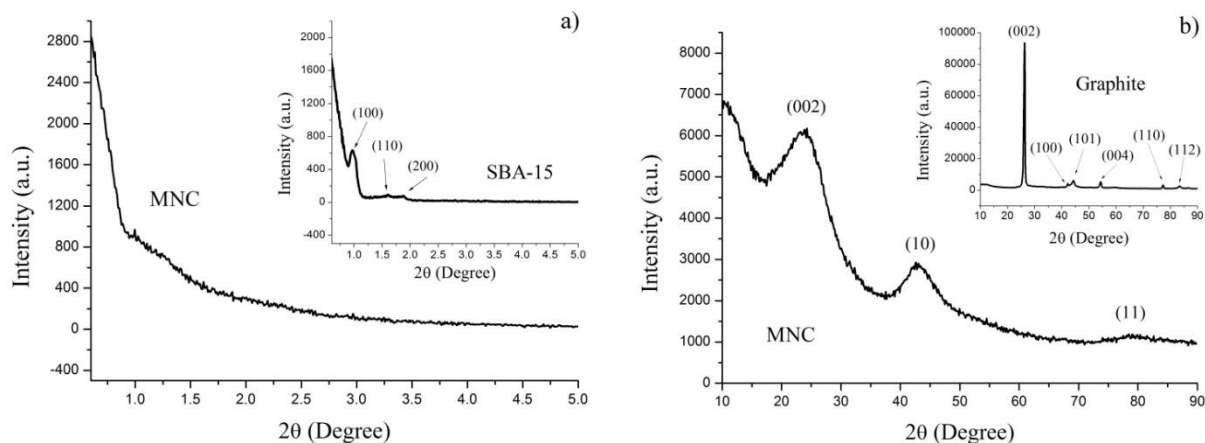


Figure 2. a) The small XRD patterns of MNC and SBA-15 (inset); b) The large XRD patterns of MNC and graphite powder (inset).

Fig. 2a shows the small XRD patterns of SBA-15 and MNC. For SBA-15, three diffraction peaks are observed at a low angle of $2\theta \sim 0.5\text{-}2.5^\circ$, which can be indexed as (100), (110), and (200) respectively, due to a highly ordered hexagonal ($p6mm$) mesostructure with a large unit cell ($a_0 = 10$ nm) [34, 42]; however, these diffraction peaks in the MNC case not appear, suggesting loss of the ordered hexagonal mesostructure perhaps due to the high temperature pyrolysis. The large XRD patterns of MNC in comparison with graphite powder in Fig. 2b are illustrated. The diffraction profile of MNC exhibit three broad bands at around 23.73° , 43.04° and 79.2° corresponding to (002), (10) and (11) peaks respectively; a shift of (002) reflection toward lower diffraction angles (in comparison with graphite at $2\theta = 26.3^\circ$) is observed. The structural parameters were calculated by means Bragg's law and Scherrer-Debye equations:

$$Lc(\text{nm}) = 0.9\lambda / (\beta_{(002)} \cos \theta_{(002)}) \tag{1}$$

$$La(\text{nm}) = 1.84\lambda / (\beta_{(100)} \cos \theta_{(100)}) \tag{2}$$

$$N = Lc / d_{(002)} \tag{3}$$

where β represent the width at half maximum intensity around at θ value, λ is the X-ray wavelength, $d_{(002)}$ is interlayer spacing between adjacent graphene layers, Lc and La represent stacking weight and crystallite lateral size of carbon particles. Table 1 shows the structural data for MNC and graphite powder.

Table 1. Structural Data from XRD patterns of MNC and graphite powder.

Sample	$\theta_{(002)}$	$d_{(002)}$	Lc	$\theta_{(10)/(100)}$	La	N
MNC	23.73°	0.3746 nm	2.039 nm	43.04°	3.738 nm	5
Graphite powder	26.31°	0.3384 nm	15.108 nm	44.2°	15.53 nm	45

Given the existence of (002) reflection and that the parameters Lc and La are smaller than those corresponding to the graphite, MNC has an intermediate structure between the amorphous coal and the

graphite, commonly denominated carbon turbostratic structure; furthermore, MNC shows a low graphitization degree. This structure is due to distortion factors such as rotation, translation, curvature, local positive fluctuation of interlayer spacing of graphene layers and fluctuation of atomic positions along the normal of graphene layers [43-47]. Raman spectroscopy has been an important tool to investigate the lattice dynamics and vibrational spectroscopy of both sp^2 and sp^3 hybridizations in carbon materials. The Raman spectra of many carbon materials show two main signatures: a G band at around 1575 cm^{-1} commonly known as graphite band related with E_{2g} phonon at the Γ point in the first Brillouin Zone of graphite and D band at around 1360 cm^{-1} related with disorder in carbon lattice attributed to a decrease in symmetry near microcrystallite edges. The intensity ratio I_D/I_G is commonly used to measure the disorder degree of carbon structures. The Tuinstra-Koenig equation:

$$L_a(\text{nm}) = 4.35(I_D / I_G)^{-1} \quad (4)$$

is usually applied in order to calculate the crystallite lateral size L_a , using intensity ratio I_D/I_G . The Fig. 3 show the Raman spectra of Suc-MNC, MNC in comparison with graphite powder (inset). The intensity ratio I_D/I_G for graphite, Suc-SBA15, MNC and were 0.32, 0.99 and 1.12 respectively, which denote the disorder degree in the carbon structures of MNC; this can explain by the coexistence of sp^2 and sp^3 hybridization states of the carbon lattice and the presence of oxygenated groups, due to the decomposition of the sucrose at 100, 160 and 1000°C . The crystallite lateral size L_a for MNC was 3.38 nm.

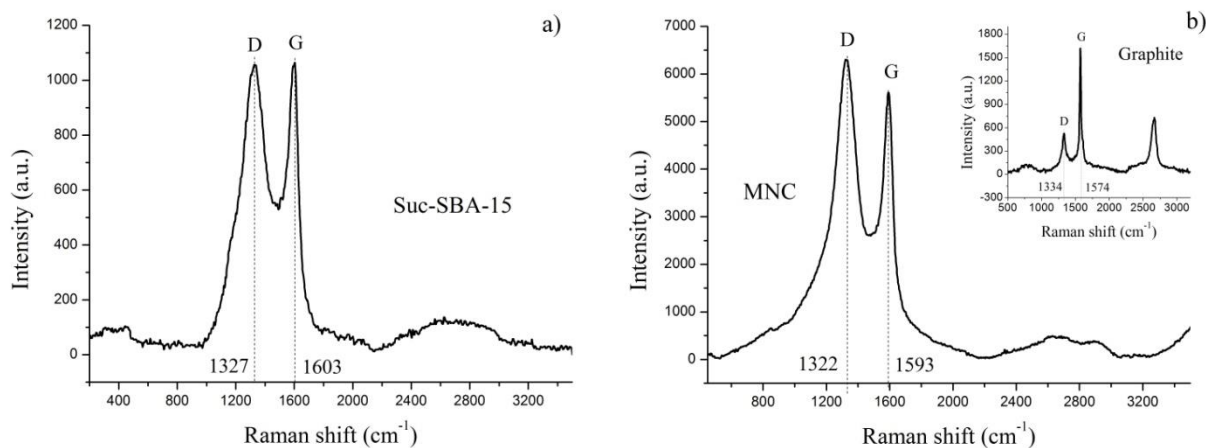


Figure 3. Raman spectra of a) Suc-SBA-15; b) MNC and graphite powder (inset)

This corroborates the existence of graphene layers with turbostratic structure of MNC [48-52], this is in accordance with XRD results.

The scanning electron microscopy with different magnifications was used to analyze the morphology of SBA-15 (hard template before carbon precursor introduction), Suc-SBA-15 (intermediate nanocomposite, after pyrolysis at 1000°C) and MNC (after removal silica process). SEM images of these materials in GB-LOW mode at 15,000X and 37,000X are shown in Fig. 4. In all cases, a rope-like morphology is present. For SBA-15 a rough grooved surface can be observed due to the open channels at the surface edges (Fig. 4a). In the case of Suc-SBA-15 nanocomposite, the grooved

surface it is still observed; furthermore, a small amount of amorphous carbon on the surface is present due to carbon that could not penetrate into the silica mesopores (Fig. 4b).

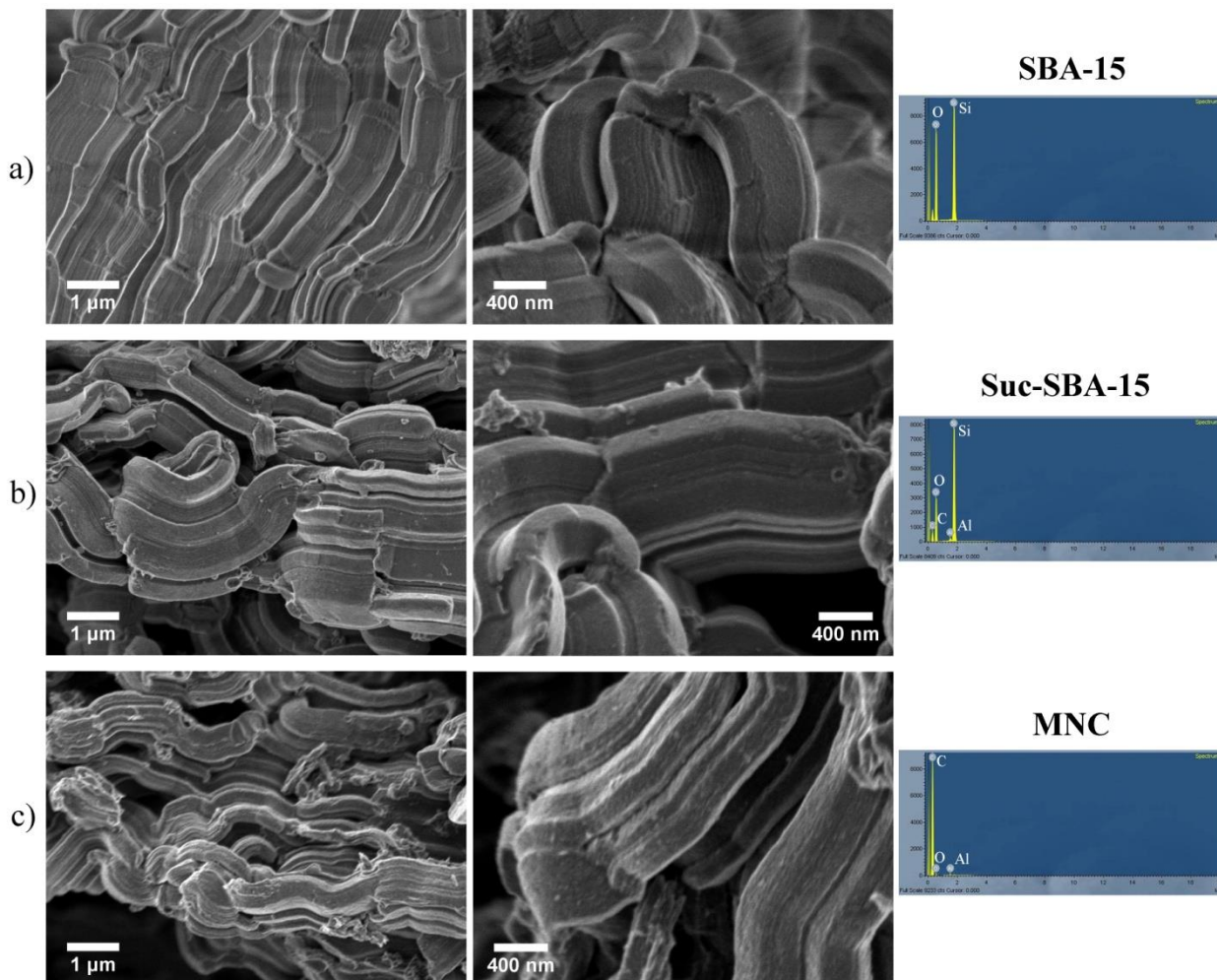


Figure 4. SEM images and EDS spectra of a) SBA-15, b) Suc-SBA-15 and c) MNC

MNC as negative replica retained the rope-like morphology after removal silica process. MNC has microstructured elements that have an average diameter of 50 μm as well as carbon nanofibers (Fig. 4c). In order to calculate the average chemical composition of materials, the energy dispersive X-ray spectroscopy was applied. EDS spectra of SBA-15, Suc-SBA15 and MNC shown in Fig. 4. The average chemical composition of SBA-15 was Si: 61.07 %wt, O: 38.93 %wt; for Suc-SBA-15, Si: 24.63 %wt, O: 47.45 %wt, C: 27.92 %wt and for MNC sample was C: 93.26 %wt, O: 6.74 which demonstrates the complete removal of silicon from the hard template. In this estimation, the aluminum used as substrate was discarded showing traces lower than 1% wt. These results are similar to those reported in the literature [53-55].

To study the morphology that cannot be visualized in scanning electron microscopy, the high resolution transmission electron microscopy technique was employed. Fig. 5 shows HRTEM images at 200 keV of SBA-15 and MNC.

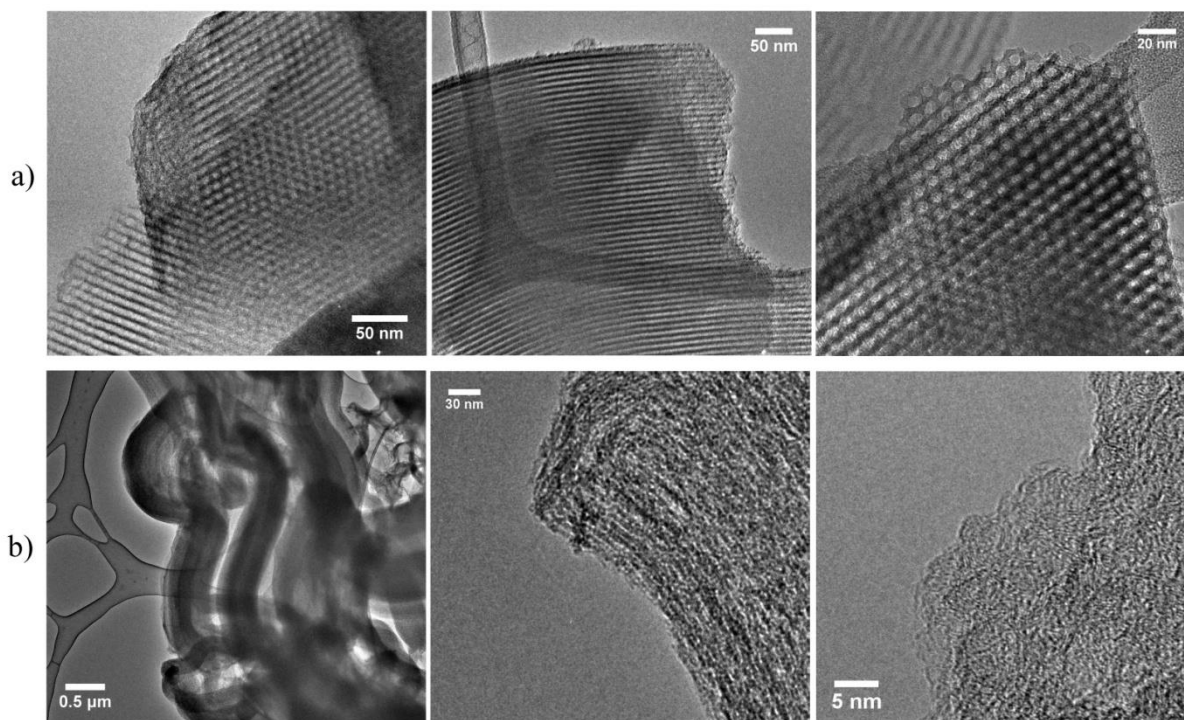


Figure 5. HRTEM images of a) SBA-15 and b) MNC

For the SBA-15 material, the channels can be observed along its microscopic and mesoscopic structure and hexagonal pore arrangement with 5-8 nm in diameter (Fig. 5a) in accordance with BJH results and with reported in literature [56-57]. For the MNC sample, an array of both nanofibers and nanopipes with a diameter in the range of (5.5-8.5) nm can be seen (Fig. 5b), in addition to graphene layers with turbostratic structure whose interlayer spacing measures approximately 0.3716 nm. This is in accordance with XRD results.

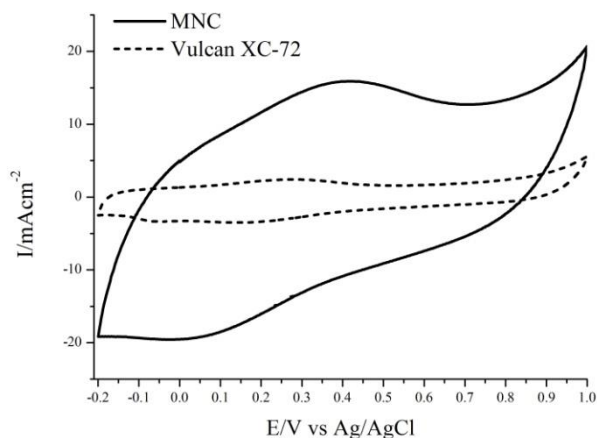


Figure 6. Cyclic voltammetry curves of MNC and Vulcan XC-72 in 0.5 M H₂SO₄ solution with a scan rate of 20 mV/s.

Cyclic voltammetry is one of the most common techniques to analyze the electrochemical performance of carbon materials. The gravimetric capacitance of MNC and Vulcan XC-72 were

calculated by integrating current in the CV curve, divided by the scan rate (mV/s), width of the potential window (V), and mass of active material (g) applied. Fig. 6 shows the cyclic voltammetry curves of the prepared carbon material MNC, and the commercial carbon black Vulcan XC-72 which also tested for comparison. According to the CV curves, the MNC carbon material shows a higher capacitance (557 F/g) compared to the commercial carbon Vulcan XC-72 (102 F/g). This may be due to the ordered mesoporous structure of MNC, the high degree of graphitization and the graphene layers that formed around the carbon nanofibers, which favors the transfer of electrons [58-59].

4. CONCLUSIONS

Micro/nanostructured carbon (MNC) was synthesized successfully according with methodology mentioned above. According with the results of characterization techniques applied, MNC is a mesoporous carbon material with large surface area and with microscopic rope-like morphology that is formed by both carbon nanofibers and carbon nanotubes that were created within the pseudo-cylindrical channels of the mesoporous material of silica SBA-15. These carbon pseudo-cylindrical elements are united by turbostratic carbon layers with small amount of amorphous carbon due to carbon that could not penetrate into the silica mesopores. In addition MNC shows good electrochemical properties as a capacitance much higher than that of commercial carbon Vulcan XC-72. Given its chemical, physical and electrochemical properties, MNC is a promising material for applications in adsorption, energy storage and solar cells, supercapacitor electrodes and electrocatalytic supports.

ACKNOWLEDGEMENTS

David Macias Ferrer gratefully acknowledges a scholarship from to National Council for Science and Technology (387542/269139) and would like to thanks for financial assistance from the National Technological Institute of Mexico/ Technological Institute of Cd. Madero (5261.14-P) Center for Research in Secondary Petrochemistry, Avenue of the Bays, Tecnia Industrial Park, Altamira Tamaulipas, México. M.C. Sebastián A. Pacheco Buendía from Research Center in Applied Science and Advanced Technology is gratefully acknowledged for performing XRD measurements.

References

1. K.S.W. Sing, D.H. Everett, R.A. W. Haul, L. Moscou, R.A. Pierotti, J. Rouquerol, T. Siemieniowska, *Pure Appl. Chem.*, 57 (1985) 603.
2. J. Rouquerol, D. Avnir, C.W. Fairbridge, D.H. Everett, J.R. Haynes, N. Pernicone, J.D.F. Ramsay, K.S.W. Sing, K.K. Unger, *Pure Appl. Chem.*, 66 (1994) 1739.
3. U. Ciesla, F. Schüth, *Microporous Mesoporous Mater.*, 27 (1999) 131.
4. W. Libbrecht, K. Vandaele, K. De Buysser, A. Verberckmoes, J.W. Thybaut, H. Poelman, J. De Clercq, P. Van Der Voort, *Mater. Basel*, 8 (2015) 1652.
5. S. Tanaka, Y. Katayama, M.P. Tate, H.W. Hillhouse, Y. Miyake, *J. Mater. Chem.*, 17 (2007) 3639.
6. L. Dai, D.W. Chang, J.-B. Baek, W. Lu, *Small*, 8 (2012) 1130.
7. Ch. Zhao, J. Li, W. Chen, Y. Yang, K. Chiang, N. Burke, *Mater. Res. Bull.*, 64 (2015) 55.
8. L. Zhu, Ch. Tian, D. Zhu, R. Yang, *Electroanalysis*, 20 (2008) 1128.
9. H.W. Kroto, J.R. Heath, S.C. O'Brien, R.F. Curl, R.E. Smalley, *Nature*, 318 (1985) 162.

10. S. Iijima, *Nature*, 354 (1991) 56.
11. S. Iijima, T. Ichihashi, *Nature*, 363 (1993) 603.
12. X.X. Wang, Z.H. Tan, M. Zeng, J.N. Wang, *Sci. Rep.*, 4 (2014) 443.
13. L. Feng, N. Xie, J. Zhong, *Mater. Basel*, 7 (2014) 3919.
14. P.-Y. Chang, K. Bindumadhavan, R.-A. Doong, *Nanomaterials*, 5 (2015) 2348.
15. Q. Ke, J. Wang, *J. Materiomics*, 2 (2016) 37.
16. R.E. Franklin, *Acta Cryst.*, 4 (1951) 253.
17. B. Manoj, A.G. Kunjomana, *Int. J. Electrochem. Sci.*, 7 (2012) 3127.
18. T. Ungár, J. Gubicza, G. Ribárik, C. Pantea, T.W. Zerda, *Carbon*, 40 (2002) 929.
19. Ch.L. Brumlik, Ch.R. Martin, *J. Am. Chem. Soc.*, 58 (1991) 1.
20. A.-H. Lu, F. Schüth, *Adv. Mater.*, 18 (2006) 1793.
21. T. Kumeria, A. Santos, D. Losic, *Sensors*, 14 (2014) 11878.
22. E. Kang, G. Jeon, J.K. Kim, *Chem Commun (Cambridge U.K.)*, 49 (2013) 6406.
23. B. Sakintuna, Z. Aktaş, Y. Yürüm, *Prepr. Pap.-Am. Chem. Soc. Div. Fuel Chem.*, 48 (2003) 614.
24. A.A. Zakhidov, R.H. Baughman, Z. Iqbal, C. Cui, I. Khayrullin, S.O. Dantas, J. Marti, V.G. Ralchenko, *Science*, 282 (1998) 897.
25. I. Muylaert, A. Verberckmoes, J. De Decker, P. Van Der Voort, *Adv. Colloid Interface Sci.*, 175 (2012) 39.
26. D. Tyagi, K. Scholz, *Int. J. Hydrogen Energy*, 37 (2012) 3602.
27. F. Hoffmann, M. Cornelius, J. Morell, M. Fröba, *Angew. Chem. Int. Ed.*, 45 (2006) 3216.
28. W. Dai, M. Zheng, Y. Zhao, Sh. Liao, G. Ji, J. Cao, *Nanoscale Res. Lett.*, 5 (2010) 103.
29. H. Wang, M. Imura, Y. Nemoto, S.-E. Park, Y. Yamauchi, *Chem. Asian J.*, 7 (2012) 802.
30. Lee J., Yoon S., Hyeon T., Oh S.M., Kim K.B., *Chem. Commun.*, 22 (1999) 2177.
31. M. Ignat, C.J. Van Oers, *Carbon*, 48 (2010) 1609.
32. N.F. Nejad, E. Shams, M.K. Amini, J.C. Bennett, *Microporous Mesoporous Mater.*, 168 (2013) 239.
33. S. Jun, S.H. Joo, R. Ryoo, M. Kruk, M. Jaroniec, Z. Liu, *J. Am. Chem. Soc.*, 122 (2000) 10712.
34. D. Zhao, Q. Huo, J. Feng, B.F. Chmelka, G.D. Stucky, *J. Am. Chem. Soc.*, 120 (1998) 6024.
35. J.P. Thielemann, F. Girgsdies, R. Schlögl, Ch. Hess, *Beilstein J. Nanotechnol.*, 2 (2011) 110.
36. R. Ryoo, S.H. Joo, S. Jun, *J. Phys. Chem. B*, 103 (1999) 7743.
37. R. Ryoo, S.H. Joo, S. Jun, T. Tsubakiyama, O. Terasaki, *Stud. Surf. Sci. Catal.*, 135 (2001) 150.
38. K.S.W. Sing, *Pure Appl. Chem.*, 54 (1982) 2201.
39. F. Azimov, I. Markova, V. Stefanova, Kh. Sharipov, *J. Univ. Chem. Technol. Metallurgy*, 47 (2012) 333.
40. A. Tadjarodi, F. Zabihi, Sh. Afshar, *Ceram. Int.*, 39 (2013) 7649.
41. N.B. Colthup, *J. Opt. Soc. Am.*, 40 (1950) 397.
42. D. Zhao, J. Feng, Q. Huo, N. Melosh, G.H. Fredrickson, B.F. Chmelka, G.D. Stucky, *Science*, 279 (1998) 548.
43. A.N. Mohan, B. Manoj, *Int. J. Electrochem. Sci.*, 7 (2012) 9537.
44. N.J. Welham, V. Berbenni, P.G. Chapman, *J. Alloy Compd.*, 349 (2003) 255.
45. X.H. Chen, H.S. Yang, G.T. Wu, M. Wang, F.M. Deng, X.B. Zhang, *J. Cryst. Growth*, 218 (2000) 57.
46. G. Zhong-min, J. Hong-zheng, Li Xiang-shan, H. Zhong, *Chem. Res. Chin. Univ.*, 19 (2003) 216.
47. B.S. Girgis, Y.M. Temerk, M.M. Gadelrab, I.D. Abdullah, *Carbon Science*, 8 (2007) 95.
48. R.L. McCreery, Y. Wang, D.C. Alsmeyer, *Chem. Mater.*, 2 (1990) 557.
49. Ch. Castiglioni, M. Tommasini, *Opt. Pura Apl.*, 40 (2007) 169.
50. L.G. Cançado, K. Takai, T. Enoki, *Appl. Phys. Lett.*, 88 (2006) 163.
51. A.C. Ferrari, D.M. Basko, *Nat. Nanotechnol.*, 8 (2013) 235.
52. F. Tuinstra, J.L. Koenig, *J. Chem. Phys.*, 53 (1970) 1126.

53. B. Babić, M. Kokunešoski, M. Miljković, B. Matović, J. Gulicovski, M. Stojmenović, D. Bučevac, *Ceram. Int.*, 39 (2013) 4035.
54. M.S. Legnoverde, S. Simonetti, E.I. Basaldella, *Appl. Surf. Sci.*, 300 (2014) 37.
55. L. Qu, J. Cai, Q. Chen, *RCS. Adv.*, 6 (2016) 14416.
56. Y. Duan, M. Zheng, D. Li, D. Deng, C Wu, Y. Yang, *RCS. Adv.*, 7 (2017) 3443.
57. V. Gascón, I. Díaz, C. Márquez-Álvarez, R.M. Blanco, *Molecules*, 19 (2014) 7057.
58. H. Kim, M.E. Fortunato, H. Xu, J. H. Bang, K.S. Suslick, *J. Phys. Chem. C*, 115 (2011) 20481.
59. H. Luo, L. Zheng, L. Lei, D. Zhang, J. Wu, J. Yang, *Korean J. Chem. Eng.*, 31 (2014) 712.

© 2018 The Authors. Published by ESG (www.electrochemsci.org). This article is an open access article distributed under the terms and conditions of the Creative Commons Attribution license (<http://creativecommons.org/licenses/by/4.0/>).